electronic reprint

Journal of
Applied Crystallography
ISSN 0021-8898

An analytical approximation for a size-broadened profile given by the lognormal and gamma distributions

N. C. Popa and D. Balzar

Journal of
Applied Crystallography
ISSN 0021-8898

Received 3 December 2001
Accepted 4 March 2002

An analytical approximation for a size-broadened profile given by the lognormal and gamma distributions

N. C. Popa[a,b] and D. Balzar[a,c]*

[a]National Institute of Standards and Technology, Boulder, CO 80305, USA, [b]National Institute for Materials Physics, PO Box MG-7, Bucharest, Romania, and [c]Department of Physics and Astronomy, University of Denver, Denver, CO 80208, USA. Correspondence e-mail: balzar@du.edu

The size-broadened profile given by the lognormal and gamma size distributions of spherical crystallites is considered. An analytical approximation for the size-broadened profile is derived that can be analytically convolved with the strain-broadened and instrumental-broadened profiles. The method is tested on two CeO_2 powders; one shows 'super-Lorentzian' profiles that were successfully modelled under the assumption of a broad lognormal size distribution. It is shown that the Voigt function, as a common model for a size-broadened profile, fails for both very narrow and broad size distributions. It is argued that the size-broadened line profile is not very sensitive to variations in size distribution and that an apparent domain size or even column-length distribution function can correspond to significantly different size distributions.

1. Introduction

There are two common approaches to extract the crystallite size and strain (here, we consider only an inhomogeneous strain associated with local distortions of the lattice arising from *e.g.* dislocations) from powder diffraction data by diffraction line-broadening analysis (LBA). One is based on the integral breadth of the diffraction lines, and gives the volume-averaged apparent dimension in the direction normal to the reflecting planes (domain size), D_V (see, for instance, a review by Klug & Alexander, 1974). The other is based on the Fourier analysis of the line profile and gives the area-averaged apparent dimension (column length) in the direction normal to the reflecting planes, D_A (Bertaut, 1949). Among the many variations of the latter approach, the Warren–Averbach method (Warren & Averbach, 1952; Warren, 1969) for the separation of size and strain contributions by Fourier analysis, is most widely used. These two crystallite-size dimensions are called 'apparent' because they only relate to the real average crystallite dimension. The second derivative of the size Fourier coefficient is related to the column-length distribution function (Warren, 1969). Presuming an identical shape for all crystallites, the column-length distribution function can be calculated as an integral with a variable limit over the crystallite distribution function (Smith, 1976). Determination of the real crystallite size distribution then includes the third derivatives of the size Fourier coefficients, which further amplifies already large initial errors of the experimental Fourier coefficients. Additionally, Fourier coefficients for large harmonic numbers are unreliable because of approximations inherent to the size–strain separation approaches (Warren, 1969; Klug & Alexander, 1974).

An unbiased determination of crystallite size and strain can be undertaken only if the diffraction lines are not overlapped. Otherwise, a pattern fitting and decomposition must be performed before any LBA can be undertaken. The fitting is performed with different degrees of constraints, the maximum number of constraints being used in the Rietveld method (Rietveld, 1969). There is ample literature on pattern decomposition and the extraction of microstructural information. Some recent reviewers include Delhez *et al.* (1993), Langford (1999), Balzar (1999), Le Bail (1999), and Louër (1999). Gauss and Lorentz (Cauchy) analytical functions are used most often in the whole-pattern fitting, with a rather loose association of strain broadening given by the former and size broadening by the latter (for a physical basis, see, for instance, Warren, 1959). Therefore, it has generally been accepted that the best profile is a convolution of the two, that is, the Voigt function. Especially, it has been shown that modeling both size-broadened and strain-broadened profiles by Voigt functions (Langford, 1980; Balzar & Ledbetter, 1993) is much more flexible and able to accommodate different sample types and deformations. Pearson VII and pseudo-Voigt functions were introduced as satisfactory approximations for the Voigt function, but being much faster to evaluate, which is of utmost importance in Rietveld refinement. Hence, one of the most used function in profile fitting is the Thompson *et al.* (1987) pseudo-Voigt function, where the full width at half-maximum (FWHM) values of the Gauss and Lorentz components are constrained to be the same and equal to the width of the pseudo-Voigt function itself.

There is no *a priori* reason to believe that a simple Voigt model can successfully describe all size- and strain-broadening-related effects in specimens. Most authors have a critical

opinion about the fitting of diffraction profiles with analytical functions such as Lorentz, Gauss or Voigt (or its approximations) functions when the main objective is the investigation of size–strain, because these profiles might correspond only to very special cases of size and strain broadening. A better approach might be the use of line profiles derived from physical models. In the past several years, much progress has been made by considering the influence of the dislocations on the strain broadening (see, for instance, Ungár *et al.*, 2001, and references therein), but only very few authors have considered the size-broadening effect. Recently, Langford *et al.* (2000) discussed the influence of normal and lognormal size distributions of spherical crystallites on the diffraction line profile. They used the numerically calculated line profiles to fit the whole diffraction pattern of nanocrystalline CeO_2. From the refined parameters, both D_V and D_A were calculated and compared with the values obtained by fitting the conventional Voigt, pseudo-Voigt and Pearson VII functions. They found good agreement for D_V, but the value of D_A depended on the fitting profile. Another important conclusion of the paper by Langford *et al.* (2000) was that the profile calculated from these physical models is intermediate between Gaussian and Lorentzian. However, they have not considered the case of large dispersion. Here, by using the same model of spherical crystallites and the lognormal distribution, we show that at very large dispersion the Voigt function or its approximations fail to describe the size-broadened profile accurately. We show that in the case of a large dispersion, the profile becomes 'super-Lorentzian', which is normally assumed to be a result of a multimodal size distribution. We derive an analytical approximation that is a sum of up to three Gauss and/or Lorentz functions that can be convoluted analytically with the strain and instrumental profile, thus facilitating implementation in the whole-pattern-fitting programs, such as Rietveld refinement programs.

The gamma distribution[1] is another bell-shaped distribution that has been used to describe the distribution of crystallite sizes (Scardi & Leoni, 2001) or crystalline defects (Berkum, 1994). We show that in this case the pseudo-Voigt function approximates well the size-broadened profile for arbitrary dispersion. Both lognormal and gamma distributions were used to fit the diffraction patterns of two CeO_2 powder samples that exhibited dominant size broadening. It is shown that for the pattern with 'super-Lorentzian' profiles, only the lognormal distribution can successfully describe the profiles, assuming a monomodal size distribution.

2. The size distribution and the line profile

The Bragg differential cross section for randomly oriented crystallites of identical shape and volume V is

$$\mathrm{d}\sigma/\mathrm{d}\Omega = V\sigma_0 P(s, \mathbf{h}), \tag{1}$$

where Ω is the solid angle, σ_0 is the unit-volume integral cross section and $P(s, \mathbf{h})$ is the line profile normalized to unit area. In $P(s, \mathbf{h})$, the variables s and $\mathbf{h}$ are

$$s = 2\sin\theta/\lambda - 1/d \quad \text{and} \quad \mathbf{h} = \mathbf{H}/H,$$

where 2θ is the scattering angle, λ is the wavelength and d is the interplanar distance corresponding to the reciprocal vector $\mathbf{H}$. The peak profile $P(s, \mathbf{h})$ can be written as

$$P(s, \mathbf{h}) = 2\int_0^\infty \psi(r, \mathbf{h}) \cos 2\pi s r \, \mathrm{d}r, \tag{2}$$

where the Fourier transform $\psi(r, \mathbf{h})$ represents the ratio between the volume common to the crystallite and its 'ghost' displaced at the distance r in the direction $\mathbf{h}$ and the crystallite volume V. It has the following properties: $\psi(0, \mathbf{h}) = 1$ and $\psi(r, \mathbf{h}) = \psi(r, -\mathbf{h})$. When the crystallites are not of identical size, the cross section must be averaged over the size distribution: $\langle \mathrm{d}\sigma/\mathrm{d}\Omega \rangle = \sigma_0 \langle VP(s, \mathbf{h}) \rangle$. Then, analogously to (1), we can define the average profile

$$\bar{P}(s, \mathbf{h}) = \langle VP(s, \mathbf{h}) \rangle / \langle V \rangle. \tag{3}$$

Now, by introducing (2) in (3) and inverting the average with the integral over r, one obtains the Fourier transform of the averaged profile:

$$\bar{\psi}(r, \mathbf{h}) = \langle V\psi(r, \mathbf{h}) \rangle / \langle V \rangle.$$

3. The isotropic case

We consider an isotropic case with spherical crystallites. Then, the size distribution f is a function only of the sphere radius R, and all defined quantities are independent of $\mathbf{h}$:

$$\psi(r) = \begin{cases} 1 - 3(r/2R)/2 + (r/2R)^3/2 & \text{for } r < 2R, \\ 0 & \text{for } r \geq 2R, \end{cases}$$

$$P(s) = (3R/2)\Phi(2\pi s R), \tag{4a}$$

$$\Phi(x) = (x^2 + \sin^2 x - x\sin 2x)/x^4, \tag{4b}$$

$$\bar{\psi}(r) = \mu_3^{-1} \int_{r/2}^\infty \mathrm{d}R \, f(R) \, (R^3 - 3R^2 r/4 + r^3/16), \tag{5}$$

$$\bar{P}(s) = (3/2\mu_3) \int_0^\infty \mathrm{d}R \, f(R) \, R^4 \Phi(2\pi s R). \tag{6}$$

In (5) and (6), μ_n is the nth moment of the distribution f.

Taking $s = 0$ in (6), one obtains the inverse of the integral breadth of the diffraction line profile in s space, which is just the volume-averaged apparent crystallite dimension (domain size):

$$\bar{P}(0) = \beta_s^{-1} = D_V = 3\mu_4/2\mu_3. \tag{7}$$

The area-averaged apparent crystallite dimension (column length) (Warren, 1969) is obtained from the initial slope of the Fourier transform of the diffraction profile. From (5) it follows that

[1] We note that the same distribution was considered previously by other authors under the name 'Poisson distribution'. Here, we follow the definition for the gamma distribution given by Abramowitz & Stegun (1964).

$$D_A = -1/\bar{\psi}'(0) = 4\mu_3/3\mu_2. \quad (8)$$

4. Application to size distributions

4.1. The lognormal distribution

The lognormal distribution for spherical crystallites is characterized by two parameters, the average radius $\bar{R}$ of the particles and the dispersion σ_R^2. It is convenient to define the dimensionless ratio

$$c = \sigma_R^2/\bar{R}^2 \quad (9)$$

to characterize the distribution. Then the lognormal distribution and its nth moment can be written as

$$f(R) = R^{-1}[2\pi \ln(1+c)]^{-1/2} \exp\left\{ -\ln^2[R\bar{R}^{-1}(1+c)^{1/2}] \times [2\ln(1+c)]^{-1}\right\}, \quad (10)$$

and

$$\mu_n = \bar{R}^n (1+c)^{(n^2-n)/2}. \quad (11)$$

By substituting (11) into (7) and (8), we find the volume- and area-averaged dimensions:

$$D_V = 3\bar{R}(1+c)^3/2 \quad (12)$$

and

$$D_A = 4\bar{R}(1+c)^2/3. \quad (13)$$

Furthermore, by introducing (10) into (5), one obtains by analytical integration:

$$\bar{\psi}(r) = (1/2)\big\{\operatorname{erfc}[v_0(r)] - (3/2)(r/2\bar{R})(1+c)^{-2}\operatorname{erfc}[v_1(r)] + (1/2)(r/2\bar{R})^3(1+c)^{-3}\operatorname{erfc}[v_3(r)]\big\}, \quad (14a)$$

where

$$v_n(r) = [2\ln(1+c)]^{-1/2}\ln[(r/2\bar{R})(1+c)^{n-5/2}] \quad (14b)$$

and

$$\operatorname{erfc}(x) = 2\pi^{-1/2}\int_x^\infty \mathrm{d}t \exp(-t^2)$$

is the complementary error function. Unfortunately, the size-broadened profile can not be calculated analytically by the Fourier transform of (14), or by direct integration of (6). For the numerical computation, the integral (6), after the introduction of (10), must be reduced to a standard quadrature formula. By using simple transformations of the integration variable, one obtains

$$\bar{P}(s) = (3\bar{R}/2)(1+c)^3\,\bar{\Phi}(2\pi s\bar{R}), \quad (15a)$$

and

$$\bar{\Phi}(x) = \pi^{-1/2}\int_{-\infty}^{\infty} \mathrm{d}t \exp(-t^2)\Phi\big(x(1+c)^{7/2}\exp\{t[2\ln(1+c)]^{1/2}\}\big). \quad (15b)$$

This integral can be computed by a standard Gauss–Hermite quadrature.

4.2. The gamma distribution

By using identically defined parameters $\bar{R}$ and c, the gamma distribution can be written as

$$f(R) = [(1/c)^{1/c}/\bar{R}\Gamma(1/c)](R/\bar{R})^{1/c-1}\exp(-R/\bar{R}c). \quad (16)$$

Though integrable for any $0 \le c < \infty$, (16) can be used as a probability distribution only for $c < 1$.

Analogous to the calculations in the previous section, we find:

$$\mu_n = (\bar{R}c)^n\Gamma(1/c+n)/\Gamma(1/c),$$

$$D_V = 3\bar{R}(1+3c)/2, \quad (17)$$

$$D_A = 4\bar{R}(1+2c)/3, \quad (18)$$

$$\bar{\psi}(r) = \chi_0(r) - (3/2)(r/2\bar{R})(1+2c)^{-1}\chi_1(r) + (1/2)(r/2\bar{R})^3(1+2c)^{-1}(1+c)^{-1}\chi_3(r), \quad (19a)$$

where

$$\chi_n(r) = \Gamma(1/c+3-n, r/2\bar{R}c)/\Gamma(1/c+3-n) \quad (19b)$$

and

$$\Gamma(a,x) = \int_x^\infty \mathrm{d}t\, t^{a-1}\exp(-t)$$

is the incomplete gamma function. Finally, the line profile follows as

$$\bar{P}(s) = (3\bar{R}/2)(1+3c)\,\bar{\Phi}(2\pi s\bar{R}), \quad (20a)$$

and

$$\bar{\Phi}(x) = [1/\Gamma(1/c+4)]\int_0^\infty \mathrm{d}t \exp(-t)t^{1/c+3}\Phi(xct). \quad (20b)$$

This integral can be computed by a standard Gauss–Laguerre quadrature, except for very small values of c, when the computation errors become significant. However, for small c, the gamma and lognormal distributions become indistinguishable [compare for example (17) with (12)], and one can use (15b) instead of (20b) to calculate $\bar{\Phi}$.

5. Determination of the distribution parameters

One can use D_V and D_A, obtained from the Fourier analysis of line profiles, to calculate values of $\bar{R}$ and c by using (12) and (13) for the lognormal distribution (Krill & Birringer, 1998) or (17) and (18) for the gamma distribution. However, except for materials with the highest crystallographic symmetry, line profiles commonly overlap, which makes it necessary to reconstruct overlapped profile tails, usually by profile fitting of simple analytical functions (Voigt or its approximations).

Another possibility to determine the size distribution parameters is to multiply (14) [or (19)] by the distortion (strain) Fourier coefficients and then fit the result to the Fourier transform of experimental diffraction profiles, corrected with the Fourier transform of the instrumental contribution (Ungár *et al.*, 2001). However, in cases of

significant profile overlapping, some way of pattern fitting also has to be used to resolve individual profiles, which is a requirement for performing the Fourier transform. Additionally, Fourier transforms of the experimental and instrumental profiles have to be calculated numerically, which introduces significant errors.

To avoid the step of pattern fitting and decomposition with simple analytical functions, Langford *et al.* (2000) proposed whole-pattern fitting with individual profiles obtained by the numerical convolutions of the size, strain and instrumental profiles in real space. Scardi & Leoni (2001) proposed to calculate the profile in the whole-pattern fitting by a numerical Fourier transform of (14) [or (19)], multiplied by the strain and the instrumental Fourier coefficients. In this way, multiple numerical integrations are avoided, all effects being accounted for in a single integral.

However, it is advantageous, especially for the Rietveld refinement, to avoid any numerical integration or necessary Fourier transform of the experimental pattern. This could be achieved if the exact size-broadened profile is accurately approximated by functions that can be analytically convolved with the strain and instrumental contributions, for instance, a combination of Gauss and Lorentz functions. However, it is not *a priori* clear whether these analytical functions give a satisfactory approximation. To illustrate this, in Fig. 1 we present $-\ln(\bar{\psi})$ calculated with (14) and (19) as a function of the variable $z = r/2\bar{R}$ for different values of c. From Fig. 1(*a*) it is obvious that the Voigt or pseudo-Voigt functions are unsatisfactory approximations of the size-broadened profile in the case of the lognormal distribution, except for small values of c. For the Voigt profile the function $-\ln(\bar{\psi})$ must be a parabola and for pseudo-Voigt it must have an asymptotic line, as can be observed in Fig. 1(*b*) for the gamma distribution. But there is no such asymptotic line if the distribution is lognormal. (Note that an asymptote $z = 1$ exists only for $c = 0$.) Alternatively, we look at the profile parameter $\phi = (\mathrm{FWHM})_\phi/\beta_\phi$, defined as the ratio between the full width at half maximum of $\bar{\Phi}$ and its integral breadth. We plot it as a function of c in Fig. 2 for both the gamma and the lognormal distribution. For the gamma distribution, the size-broadened profile is between a Gaussian and a Lorentzian for any c. Contrarily, for the lognormal distribution, $\bar{\Phi}(x)$ decreases with increasing x much slower than a Lorentzian, except for small values of c. But, for a finite range of x, the profile could be fairly described if more Lorentzian functions were added. This will be discussed in the next section.

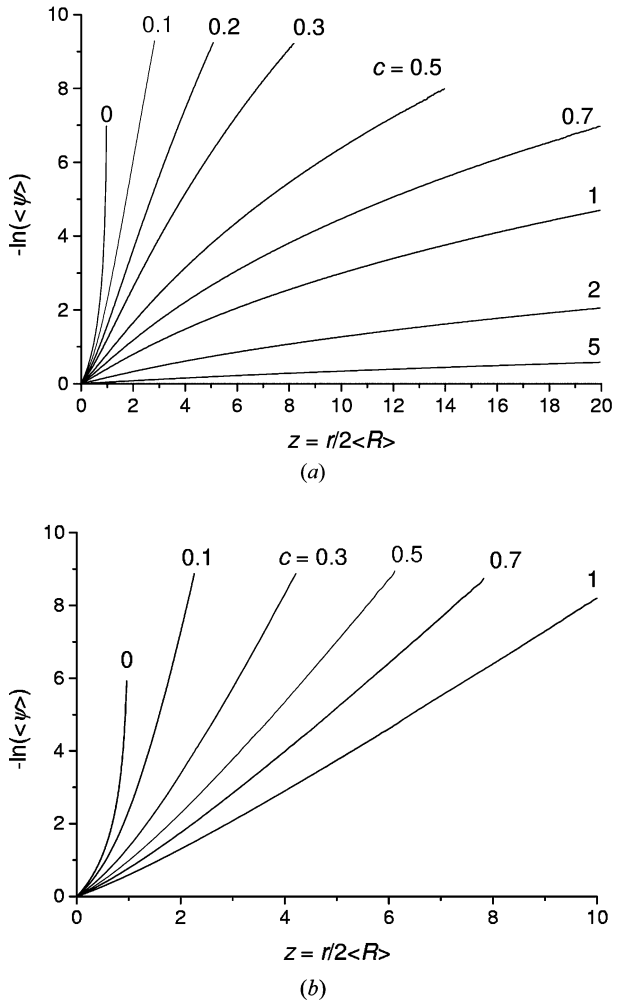

Figure 1
$-\ln(\bar{\psi})$ as a function of $z = r/2\bar{R}$ for different values of c: (*a*) calculated with (14) for the lognormal distribution; (*b*) calculated with (19) for the gamma distribution.

6. The analytical approximation for $\bar{\Phi}(x)$

6.1. The lognormal distribution

The function $\bar{\Phi}(x)$ given by (15*b*) has been calculated numerically at equal steps in x in the range $1 \geq \bar{\Phi} > 10^{-2}$ by a Gauss–Hermite quadrature with 16 nodes for 53 values of c in the interval [0, 6]. These exact profiles were least-squares fitted by linear combinations of Gauss and Lorentz functions. The following combination was found to be a good approximation for c in the interval [0, 6]:

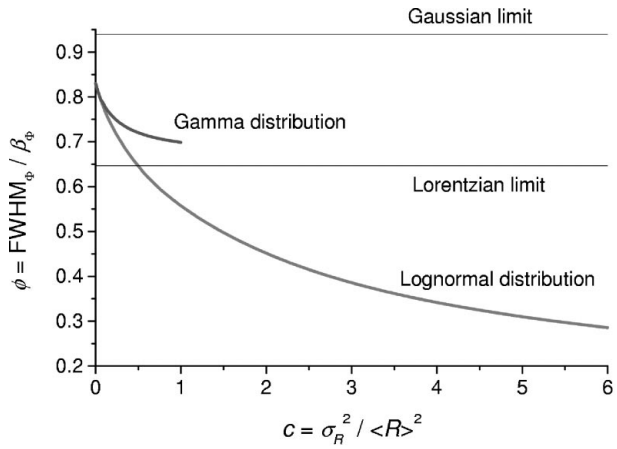

Figure 2
The profile parameter as a function of c for spherical crystallites, lognormal and gamma distributions.

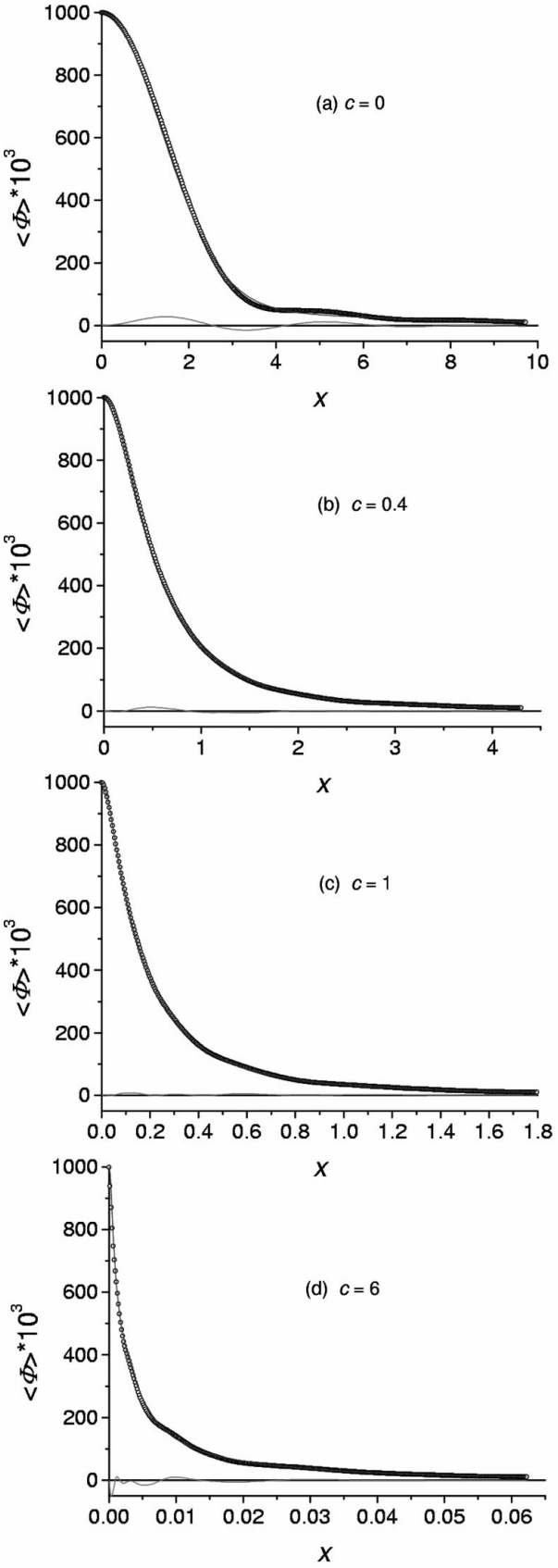

Figure 3
The function $\bar{\Phi}(x)$ for the lognormal distribution at four values of the parameter c. The points are the exact values and the solid line is the fit by (21). The difference curve between the exact and fitted values is also shown.

$$\bar{\Phi}(x) = (8/3)(1+c)^{-3}\left[\eta_1 a_1^{-1}(1+4x^2/a_1^2)^{-1} + \eta_2 a_2^{-1}(1+4x^2/a_2^2)^{-1} + (1-\eta_1-\eta_2)a_3^{-1}\begin{cases}\exp(-4x^2/\pi a_3^2) & \text{for } c \le 1\\ (1+4x^2/a_3^2)^{-1} & \text{for } c > 1\end{cases}\right]. \quad (21a)$$

The parameters η_1, a_1, η_2, a_2 ($0 \le \eta_i \le 1$) were freely adjusted during the fit but a_3 was constrained to conserve the integral breadth of the exact profile:

$$a_3 = (1-\eta_1-\eta_2)/[3(1+c)^3/8 - \eta_1/a_1 - \eta_2/a_2]. \quad (21b)$$

Further, the parameters η_1, a_1, η_2, a_2 were fitted by empirical analytical functions in c:

$$\eta_1(c) = 0.25631 + 0.018638c + 0.001155c^2 + 3.5671c\exp(-2.0467c^{0.93346}), \quad (22a)$$

$$a_1(c) = 4.02326\exp(-44.6429c) + 3.13982\exp(-7.01128c) + 0.580742\exp(-0.413958c) + 0.381245\exp(-1.10827c), \quad (22b)$$

$$\eta_2(c) = \begin{cases} 0 & \text{for } c \le 0.4,\\ 0.59951 - 0.020058(c-0.4) - 0.45347/[1+3.3933(c-0.4)^2] & \\ \quad -0.14604\exp[-0.49272(c-0.4)^2] & \text{for } c > 0.4,\end{cases} \quad (22c)$$

$$a_2(c) = 0.32781[1 + 1.5399(c-0.4) - 0.21223(c-0.4)^2 + 0.18158(c-0.4)^3]^{-1}. \quad (22d)$$

As can be seen from (21*a*) and (22*c*), the pseudo-Voigt function is a satisfactory approximation for the size-broadened profile only for $c \le 0.4$. For higher value of c, a second Lorentz function must be added. Its weight increases with increasing c and the weight of the Gauss component decreases. For $c \simeq 1$, the profile is well approximated by a sum of two Lorentz functions. A third Lorentz function must be added for $c > 1$. For $c > 6$, even three Lorentz functions are not enough for a satisfactory fit, but it is highly unlikely to find samples with such a large dispersion of crystallite sizes. The exact $\bar{\Phi}$ and its approximation by (21) in the range Δx for which $1 \ge \bar{\Phi} > 10^{-2}$ are shown in Fig. 3 for four values of c. The decrease of the ratio of the FWHM and Δ (taken as a measure of the tail length) with c can be easily observed.

6.2. The gamma distribution

A Gauss–Laguerre quadrature with eight nodes was used to compute $\bar{\Phi}(x)$ given by (20*b*) in the segment $c \in [0, 1]$ with the step $\Delta c = 0.05$ under conditions similar to those for the lognormal distribution. Furthermore, the computed profiles were least-squares fitted with the following pseudo-Voigt function:

$$\bar{\Phi}(x) = (8/3)(1+3c)^{-1}[\eta a_1^{-1}(1+4x^2/a_1^2)^{-1} + (1-\eta)a_2^{-1}\exp(-4x^2/\pi a_2^2)], \quad (23a)$$

where a_2 was constrained to conserve the integral breadth:

$$a_2 = (1-\eta)/[3(1+3c)/8 - \eta/a_1]. \quad (23b)$$

Finally, we have found the following empirical expressions for η and a_1:

$$\eta(c) = 1 - [0.407597\exp(-7.752c) + 0.336093\exp(-0.633744c)] \quad (24a)$$

and

$$a_1(c) = 4.98231\exp(-27.1875c) + 1.75734\exp(-4.86798c) + 1.38542\exp(-0.736325c). \quad (24b)$$

7. Application to two powder samples

We tested the model of spherical crystallites distributed according to the lognormal and gamma size distributions on two CeO_2 powder samples. Sample 1 was prepared for the Commission on Powder Diffraction (CPD) Size–Strain Round Robin (see Audebrand *et al.*, 2000; Balzar, 2001), and sample 2 is a commercially available CeO_2 powder (Nanotech[2]). A third sample was prepared from sample 2 by annealing at 1573 K for 3 h, followed by slow cooling in the furnace, to determine the instrumental broadening. A comparative analysis with NIST SRM660 LaB_6 as an instrumental standard gave almost identical results (within a single standard uncertainty). The X-ray diffraction patterns were collected using a commercial diffractometer in Bragg–Brentano geometry with Cu $K\alpha_{1,2}$ radiation. For every sample, three diffraction patterns were collected, at low (20–64.5° in 2θ, 0.01° step, 10 s step^{-1} for the annealed sample, and 0.02° step, 65 s step^{-1} for broadened patterns), medium (64.5–102° in 2θ, 0.02° step, 25 s step^{-1} for the annealed sample, and 0.04° step, 130 s step^{-1} for broadened patterns), and high (102–150° in 2θ, 0.02° step, 30 s step^{-1} for the annealed sample, and 0.05° step, 160 s step^{-1} for broadened patterns) diffraction angles, to obtain comparable statistics. The diffraction patterns of the two samples show very different line profiles (see Fig. 4). Sample 1 shows 'regularly' broadened lines with $K\alpha_1$ and $K\alpha_2$ overlapped at high angles, which can be successfully fitted by the Voigt function or its approximations, while sample 2 exhibits 'super-Lorentzian' profiles, with long tails and $K\alpha_1$ and $K\alpha_2$ separated at high angles.

Profiles of the annealed sample were corrected for the Lorentz–polarization factor and fitted by a sum of four Voigt functions resulting from the convolution of a Gaussian, modeling geometrical broadening with four Lorentzians representing the spectral profile of the Cu $K\alpha_1$–$K\alpha_2$ line. The wavelengths and weights of four Lorentzians were taken from the literature (Holzer *et al.*, 1997). The integral breadth, constant background, profile position and intensity were adjusted in the least-squares refinement. All profiles gave values of integral breadths within one standard uncertainty except for four lines at low angles, which are affected by asymmetry. To avoid systematic errors, the results from the first pattern at low diffraction angles were not included in the subsequent analysis.

Approximations (21) and (22) for the lognormal, and (23) and (24) for the gamma distribution were used to model the size-broadened profile. Although at least sample 1 shows negligible strain broadening (Audebrand *et al.*, 2000), we allowed for a small strain correction by convolving the size-broadened profile with a Gaussian and with the instrumental profile. Therefore, every line profile was a sum of up to 12 Voigt functions for the lognormal distribution and eight for the gamma distribution. The two diffraction patterns at medium and high diffraction angles were least-squares fitted independently. The free parameters were the intensity and position for every profile, and the global parameters included two background parameters, the size-distribution parameters $\bar{R}$, c and the Gaussian strain parameter. For sample 1, the strain parameter was fixed to zero as we did not see any improvement in the fit. For sample 2, the strain parameter, although very small [$\langle\varepsilon^2\rangle^{1/2}$ = 0.00033 (1)], improved the fit slightly.

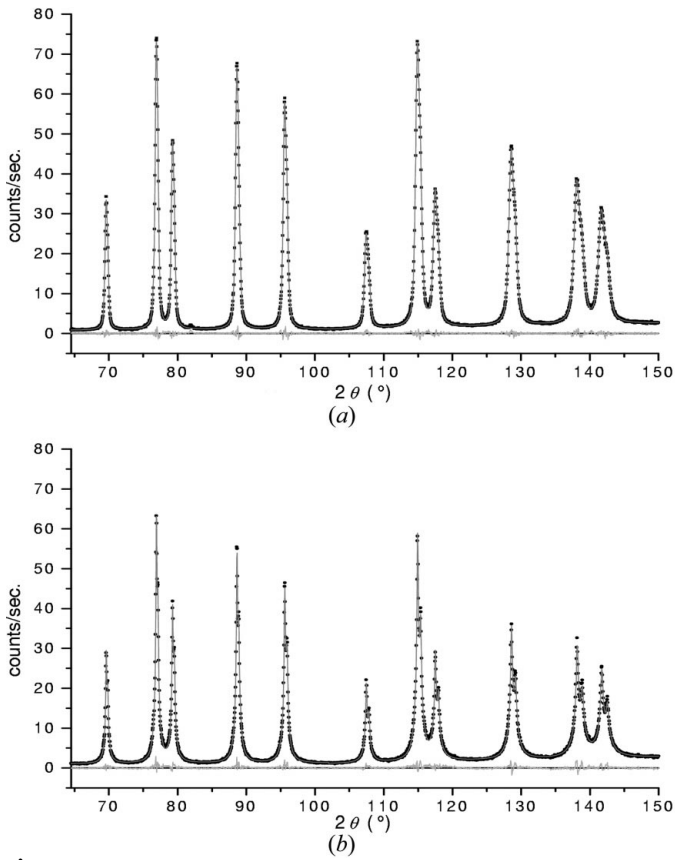

Figure 4
The CeO_2 powder pattern fitted with the size-broadened profile calculated by (15*a*) and (21*a*) for the lognormal distribution: (*a*) sample 1, R_{wp} = 0.0390; (*b*) sample 2, R_{wp} = 0.0477.

[2] Commercial names are given for identification purposes only.

Table 1
The results of the fit for samples 1 and 2.

The average radius $\bar{R}$, volume-averaged D_V, and area-averaged D_A apparent domain sizes are given in Å units. Because of a poor fit, the values for sample 2 with gamma size distribution are not given.

	Sample 1				Sample 2			
Distribution	$\bar{R}$	c	D_V	D_A	$\bar{R}$	c	D_V	D_A
Lognormal	89.7 (6)	0.181 (4)	222 (3)	167 (2)	16.8 (2)	2.820 (2)	1408 (14)	328 (3)
Gamma	69 (1)	0.39 (1)	224 (5)	164 (3)				

The fit results for the lognormal distribution are shown in the Fig. 4. For clarity, we plot both medium- and high-angle diffraction patterns together, although they were fitted independently. As can be seen from the difference plots and reliability factors, the diffraction patterns were fitted with similar reliability using lognormal and gamma distributions (compare Figs. 4 and 5). The fit with the gamma distribution was even slightly better for sample 1 (Fig. 5*a*), but clearly inadequate for sample 2 (Fig. 5*b*). For the latter, the gamma distribution cannot model the size-broadened profile to yield a 'super-Lorentzian', in accord with the theoretical discussion in the preceding paragraphs. The numerical results are summarized in Table 1. The reported values are the average of the refined values obtained by independent fitting of the two diffraction patterns at medium and high diffraction angles.

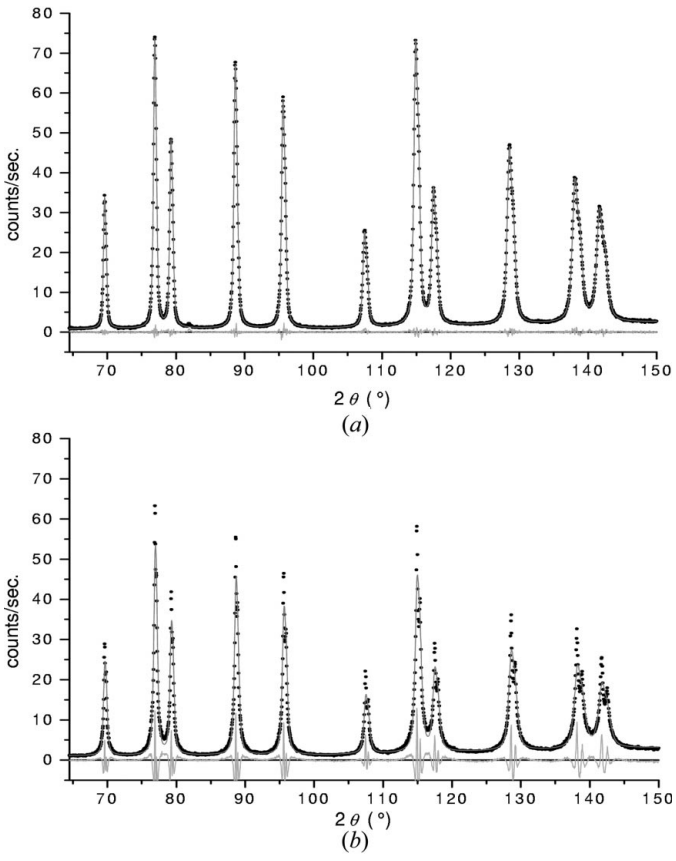

Figure 5
The CeO_2 powder pattern fitted with the size-broadened profile calculated by (20*a*) and (23*a*) for the gamma distribution: (*a*) sample 1, $R_{wp} = 0.0375$; (*b*) sample 2, $R_{wp} = 0.1435$.

Two details worth noting are as follows. First, the 'super-Lorentzian' profile of sample 2 results in the large value of the c parameter. Second, sample 1 gives significant differences in both $\bar{R}$ and c parameters for the two distributions, but the corresponding values of D_V and D_A differ by only 1.12 and 1.68%, respectively. In the Fig. 6(*a*), we present the distributions calculated with the parameters $\bar{R}$ and c from the Table 1. The curves 1 and 2 are the lognormal and the gamma size distributions, respectively. Although they have similar shape, there is a significant difference that could be a basis for discrimination if other data (such as transmission electron microscopy data) are available.

The results obtained for sample 1 implicate that significantly different size distributions can give practically indistinguishable diffraction profile. Because the profile is an integral over the distribution, relatively large variations in integrand can still give small variation in the result of integration. In other words, the diffraction profile is insensitive to the details of the

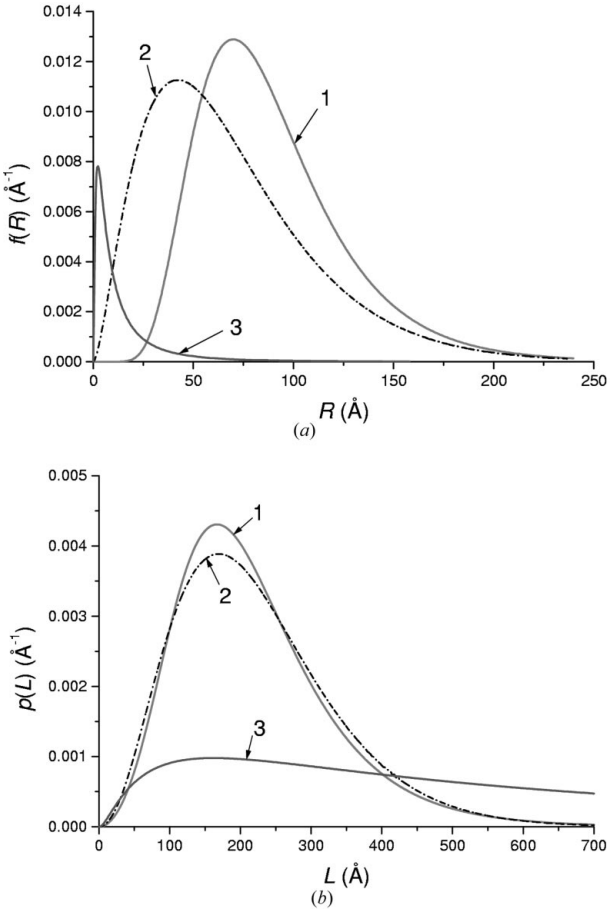

Figure 6
The distribution functions of the crystallite radius (*a*) and column length (*b*) calculated with the parameters $\bar{R}$ and c, as obtained from the fit of CeO_2 diffraction patterns: (1) sample 1, lognormal distribution; (2) sample 1, gamma distribution; (3) sample 2, lognormal distribution. In (*a*) the curve (3) was multiplied by 10^{-1}. In (*b*), only 50% of the area under curve (3) is shown in the given range.

distribution. One can obtain values for D_V and D_A that well fit the diffraction pattern, but do not yield significant physical information about the actual crystallite-size distribution. Although to a somewhat smaller degree, the column-length distribution function, which is commonly extracted from the Warren–Averbach (1952) type of analysis, is also relatively insensitive to the crystallite-size distribution. To illustrate this, we calculate the volume-averaged column-length distribution function from the second derivative of the Fourier coefficients (Guinier, 1963):

$$p(L) = L(\mathrm{d}^2\bar{\psi}/\mathrm{d}r^2)_{r=L} = (3L^2/8\mu_3)\int_{L/2}^{\infty} \mathrm{d}R f(R)$$
$$= \begin{cases} [3L^2/16\bar{R}^3(1+c)^3]\,\mathrm{erfc}\,[v_3(L)] & \text{for the lognormal distribution,} \\ [3L^2/8\bar{R}^3(1+2c)(1+c)]\chi_3(L) & \text{for the gamma distribution.} \end{cases}$$

Fig. 6(*b*) shows column-length distribution functions corresponding to the size distribution functions from Fig. 6(*a*). The curves 1 and 2 differ in the position of the maximum by only 2 Å and in height of the maximum by 9.76%.

8. Summary and concluding remarks

We have shown that the size-broadened line profiles can be satisfactorily modeled by an *a priori* size distribution. In particular, we have discussed two widely used distributions: lognormal and gamma. An important difference between the lognormal and gamma distributions is that the former can model a much wider range of actual crystallite-size dispersions found in practice. We have shown that the so-called 'super-Lorentzian' profiles can be explained by a broad size distribution. The line profiles of a commercial CeO_2 powder that showed tails falling off more slowly than the Lorentzian function were successfully fitted on the assumption of a broad lognormal size distribution, but not by using the gamma distribution. We avoided the need to convolute numerically either the size-broadened profile with the strain and instrumental profiles or the numerical Fourier transforms by approximating the size-broadened profile by simple analytical functions that can be analytically convolved.

We found that the size-broadened profile can be approximated by a pseudo-Voigt function, which is commonly used in Rietveld refinement programs, only for samples with a limited dispersion in the region $0 \leq c \leq 0.4$ for the lognormal distribution, and in the region $0 \leq c < 1$ for the gamma distribution. It is worthwhile noting here that the gamma distribution in the region $0 \leq c < 1$ does not yield Lorentzian-like size profiles, as is evident from Fig. 2. Consequently, a commonly used approximation of a size profile by a Lorentzian is incompatible with an assumed gamma crystallite-size distribution. From §3, it follows that for the lognormal distribution the ratio $D_V/D_A = (9/8)(1+c)$ can take values in the range $[1.125, \infty)$, and for the gamma distribution the same ratio $D_V/D_A = (9/8)(1+3c)/(1+2c)$ can take values in the range [1.125, 1.5). The size-broadened profile is very often modeled by the Voigt function. It was found (Balzar & Ledbetter, 1993) that the size-broadened Voigt function requires the ratio of volume-averaged and area-averaged domains to be in the range [1.31, 2) in order for the column-length distribution function to be positive. The lower limit of this ratio constrain the dispersion parameter, $c \geq 0.164$ for the lognormal distribution and $c \geq 0.245$ for the gamma distribution. Therefore, the Voigt function appears to be an inadequate approximation for very sharp lognormal and gamma size distributions and a broad lognormal distribution of spherical crystallites! These additional restrictions are not placed on a pseudo-Voigt function, which indicates that the latter might be a better approximation for the size-broadened profile for samples with narrow crystallite-size distributions. The fact that the pseudo-Voigt and particularly the Voigt function are found satisfactory in most cases probably indicates that most powders fall within a relatively narrow range of dispersion for both lognormal and gamma distributions.

Lastly, we argue that in principle, diffraction does not yield enough information to determine the crystallite-size distribution. Diffraction line-broadening analysis yields only the parameters of an *a priori* size model, either through a phenomenological approach (Voigt, pseudo-Voigt or other arbitrary chosen analytical functions) or through a physically based model, such as lognormal or gamma distribution of spherical crystallites. Although the latter approach can explain 'super-Lorentzian' line profiles, as it was shown in the case of a broad lognormal distribution, the 'super-Lorentzian' line profiles can be alternatively explained by a multimodal size distribution. Therefore, additional information, preferably obtained by an unrelated method such as transmission electron microscopy, is necessary to give an unequivocal determination of the size distribution, although this is not easy to achieve by any experimental method in the case of a broad distribution with a large percentage of small crystallites, such as our sample 2. Contrarily, if the measured crystallite-size distribution is narrow, it is difficult to discern which bell-shaped function gives a better fit.

We gratefully acknowledge Nathalie Audebrand and Daniel Louër (University of Rennes), for preparing the CeO_2 powder, and the Commission on Powder Diffraction (CPD) of the International Union of Crystallography (IUCr) for supporting the Size–Strain Round Robin.

References

Abramowitz, M. & Stegun, I. A. (1964). *Handbook of Mathematical Functions*, p. 930. Washington, DC: National Bureau of Standards.
Audebrand, N., Auffrédic, J.-P. & Louër, D. (2000). *Chem. Mater.* **12**, 1791–1799.
Balzar, D. (1999). In *Defect and Microstructure Analysis by Diffraction*, edited by R. Snyder, J. Fiala & H. J. Bunge, pp. 94–126. IUCr/Oxford University Press.
Balzar, D. (2001). http://www.boulder.nist.gov/div853/balzar/.
Balzar, D. & Ledbetter, H. (1993). *J. Appl. Cryst.* **26**, 97–103.
Berkum, J. G. M. van (1994). PhD thesis, Delft University of Technology, p. 136.

Bertaut, E. F. (1949). *C. R. Acad. Sci. Paris*, **228**, 187–189.
Delhez, R., de Keijser, T. H., Langford, J. I., Louër, D., Mittemeijer, E. J. & Sonneveld, E. J. (1993). In *The Rietveld Method*, edited by R. A. Young, pp. 132–166. IUCr/Oxford University Press.
Guinier, A. (1963). *X-ray Diffraction*, p. 139. San Francisco: Freeman.
Holzer, G., Fritsch, M., Deutsch, M., Hartwig, J. & Forster, E. (1997). *Phys. Rev. A*, **56**, 4554–4568.
Klug, H. P. & Alexander, L. E. (1974). *X-ray Diffraction Procedures*, 2nd ed. New York: John Wiley.
Krill, C. E. & Birringer, R. (1998). *Philos. Mag. A*, **77**, 621–640.
Langford, J. I. (1980). In *Accuracy in Powder Diffraction*, *Natl Bur Stand. Spec. Publ. No. 567*, pp. 255–269.
Langford, J. I. (1999). In *Defect and Microstructure Analysis by Diffraction*, edited by R. Snyder, J. Fiala & H. J. Bunge, pp. 59–81. IUCr/Oxford University Press.
Langford, J. I., Louër, D. & Scardi, P. (2000). *J. Appl. Cryst.* **33**, 964–974.
Le Bail, A. (1999). In *Defect and Microstructure Analysis by Diffraction*, edited by R. Snyder, J. Fiala & H. J. Bunge, pp. 535–555. IUCr/Oxford University Press.
Louër, D. (1999). In *Defect and Microstructure Analysis by Diffraction*, edited by R. Snyder, J. Fiala & H. J. Bunge, pp. 673–697. IUCr/Oxford University Press.
Rietveld H. (1969). *J. Appl. Cryst.* **2**, 65–71.
Scardi, P. & Leoni, M. (2001). *Acta Cryst.* A**57**, 604–613.
Smith, W. L. (1976). *J. Appl. Cryst.* **9**, 187–189.
Thompson, P., Cox, D. E. & Hastings, J. B. (1987). *J. Appl. Cryst.* **20**, 79–83.
Ungár, T., Gubicza, J., Ribárik, G. & Borbély, A. (2001). *J. Appl. Cryst.* **34**, 298–310.
Warren, B. E. (1959). In *Progress in Metal Physics*, Vol. 8, edited by B. Chalmers & R. King, pp. 147–202. New York: Pergamon.
Warren, B. E. (1969). *X-ray Diffraction*, pp. 251–314. New York: Addison-Wesley.
Warren, B. E. & Averbach B. L. (1952). *J. Appl. Phys.* **23**, 497.